Reservoir Simulation With a Control-Volume Finite-Element Method

L.S.-K. Fung, SPE, **A.D. Hiebert,** SPE, and **L.X. Nghiem,** SPE, Computer Modelling Group

Summary. This paper describes a control-volume finite-element (CVFE) method incorporating linear triangular elements for the simulation of thermal multiphase flow in porous media. The technique adopts the usual finite-element shape functions to evaluate flow potentials at the control-volume boundaries and uses the conservation equations for each control volume. The main advantage of the CVFE method over the finite-difference method is in the representation of complex reservoir geometries. In addition, desirable features, such as local grid refinement for near-well resolution, can be achieved simply and consistently. The control-volume approach enforces local mass conservation and permits a direct physical interpretation of the resulting discrete equations. These are significant advantages over the classical Petrov-Galerkin or variational finite-element methods. The method was implemented in a general-purpose thermal simulator. Numerical examples compare the proposed method with five-point and nine-point finite-difference schemes in terms of grid-orientation effects and run time. The CVFE method was found to reduce grid-orientation effects significantly. At the same time, computational cost was much lower than for the nine-point scheme. The geometric flexibility of the method also is demonstrated.

Introduction

In many reservoir simulation problems, a flexible discretization method is extremely useful in the definition of complex reservoir geometries and discontinuities (such as faults) and in enhancing the resolution near the wells. The use of Cartesian grids with finite-difference methods has created difficulties and/or complexities in the definition of complex geometries or grid refinements.[1-6] It is desirable to adopt the intrinsic grid flexibility of the finite-element method. However, combining upstream weighting with the usual finite-element method for the multiphase multidimensional flow problem presents difficulties. Although asymmetric weighting procedures like the Petrov-Galerkin method[7] have been introduced to deal with the convective terms in the mixed convective-diffusive flow problems, such methods are in general not mass-conservative in the local sense. On the other hand, local mass conservation is a specific requirement of the control-volume methods. In addition, reservoir simulation problems can be very complex, involving multiphase mass and heat flow with interphase transfers and chemical reactions. The mass-conservative aspect of the control-volume methods is a distinct advantage in the programming and testing of these simulators.

The CVFE method was proposed in computational fluid dynamics for solving the Navier-Stokes equations,[8,9] where flexible gridding and local mass, momentum, and energy conservation are achieved. In this paper, a CVFE procedure for the reservoir flow equations is developed where flexible grid geometry is obtained without sacrificing the advantageous attributes of the control-volume finite-difference method. The derivation shows that the use of the perpendicular-bisection[10] grid and the seven-point finite-difference method[11] are special cases of this discretization method. Recently, Forsyth[12] applied a CVFE method to the local-mesh-refinement problem by providing a smooth transition between the coarse and fine grids. As discussed in detail later, a proper choice of the triangular finite-element mesh is crucial to the reduction of grid-orientation effects. The construction of a CVFE grid by triangulation with one of the diagonals of each rectangle in a Cartesian grid (as in Ref. 12) will result in a five-point discretization scheme because the diagonal flow terms for this grid are identically equal to zero.

The method results in a set of discretized conservative equations where the Jacobian construction for Newton's method and the upstream weighting of mobilities can be done in the usual way. For the incompressible single-phase flow problem, the method gives the same stiffness matrix as the Petrov-Galerkin weighted-residual finite-element method when linear shape functions are used. The criterion for maintaining positive transmissibility coefficients of a general anisotropic system also is derived. A number of examples are included to demonstrate the geometric flexibility, non-grid-orientation characteristics, and efficiency of the proposed method.

CVFE Method

Discretization. To examine the discretization process with CVFE, we use the integrated form of the transport equation in porous media:

$$\int_V \frac{\partial}{\partial t}(\phi\rho)\mathrm{d}V = \int_V \nabla\cdot(k\nabla\Phi)\mathrm{d}V. \quad \ldots\ldots\ldots\ldots\ldots\ldots\ldots\ldots (1)$$

Applying the Gauss divergence theorem with a lump mass approach to the accumulation term gives

$$V_b\frac{(\phi\rho)^{n+1}-(\phi\rho)^n}{\Delta t} = \int_s k\nabla\Phi\cdot\vec{n}\,\mathrm{d}s. \quad \ldots\ldots\ldots\ldots\ldots\ldots\ldots\ldots (2)$$

The integral in Eq. 2 is a surface integral over all the edges of the control volume (see **Fig. 1**). The calculation of the flow terms on an elemental basis is given in the following. Consider **Fig. 2** and let γ be a point inside the triangular element $\gamma\epsilon\Delta_{123}$. The control-volume boundaries, e_1, e_2, and e_3 are constructed by joining γ to the midpoint of each of the triangle's sides. The flow term for Subcontrol Volume 1 involves the flux across the volume boundaries e_2 and e_3; i.e.,

$$u_1 = -\int_{e_2+e_3} k\nabla\Phi\cdot\vec{n}\,\mathrm{d}s$$

$$= -\int_{e_2+e_3} k_x\frac{\partial\Phi}{\partial x}\mathrm{d}y - k_y\frac{\partial\Phi}{\partial y}\mathrm{d}x. \quad \ldots\ldots\ldots\ldots\ldots\ldots\ldots\ldots (3)$$

To evaluate the terms in Eq. 3, consider the triangular element in **Fig. 3,**

$$a_k = x_{ji} = x_j - x_i,\ i, j, k = 1,2,3 \quad \ldots\ldots\ldots\ldots\ldots\ldots\ldots\ldots (4a)$$

and $$b_i = y_{jk} = y_j - y_k,\ i, j, k = 1,2,3, \quad \ldots\ldots\ldots\ldots\ldots\ldots\ldots\ldots (4b)$$

where a_k and b_i are obtained from the anticyclic permutation of x and the cyclic permutation of y, respectively. From **Fig. 4,** it can easily be seen that the linear interpolation functions for the element are

$$N_i = \frac{\eta_i}{h_i} = \frac{A_i}{A},\ i = 1,2,3, \quad \ldots\ldots\ldots\ldots\ldots\ldots\ldots\ldots (5)$$

where A_i are the areas of the triangles in the element and A is the total area, such that

$$A = \sum_{i=1}^{3} A_i. \quad \ldots\ldots\ldots\ldots\ldots\ldots\ldots\ldots (6)$$

Any variable in the element Δ_{123} may be defined if the nodal values of the variable are known. For example,

$$\Phi = \sum_{i=1}^{3} N_i\Phi_i. \quad \ldots\ldots\ldots\ldots\ldots\ldots\ldots\ldots (7)$$

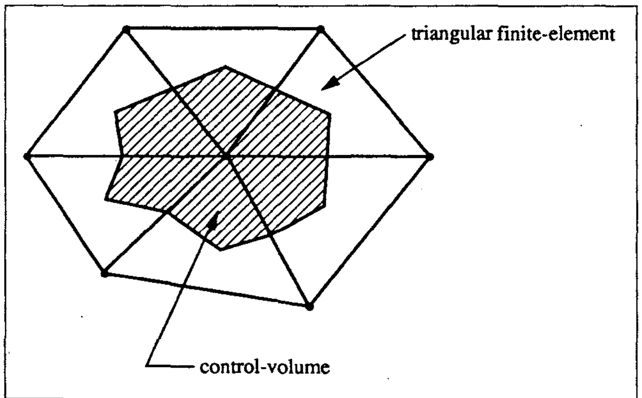

Fig. 1—A control volume in the triangular finite-element mesh.

From simple geometry, one can show that the derivatives of N_i with respect to x and y are

$$\frac{\partial N_i}{\partial x}=\frac{b_i}{2A} \quad \text{(8a)}$$

and $$\frac{\partial N_i}{\partial y}=\frac{a_i}{2A}. \quad \text{(8b)}$$

In matrix form, for a variable Φ,

$$\left\{\frac{\partial \Phi}{\partial x_j}\right\}=\left[\frac{\partial N_i}{\partial x_j}\right]\{\Phi_i\}, \quad \begin{matrix} i=1,2,3 \\ j=1,2 \end{matrix}, \quad \text{(9)}$$

where $$\left[\frac{\partial N_i}{\partial x_j}\right]=\frac{1}{2A}\begin{bmatrix} b_1 & b_2 & b_3 \\ a_1 & a_2 & a_3 \end{bmatrix}=\frac{1}{2A}[B]. \quad \text{(10)}$$

It is important to note that, for the linear interpolation function N_i, the $[B]$ matrix is a constant-coefficient matrix; i.e., the derivatives $\partial N_i/\partial x$, $\partial N_i/\partial y$ are constants within the element. Returning to Eq. 3, if k_x and k_y are constant along e_2 and e_3, we get

$$u_1=-\left[\frac{k_x}{4A}\left(\sum_{i=1}^{3} b_i\Phi_i\right)(b_2+b_3) + \frac{k_y}{4A}\left(\sum_{i=1}^{3} a_i\Phi_i\right)(a_2+a_3)\right]. \quad \text{(11)}$$

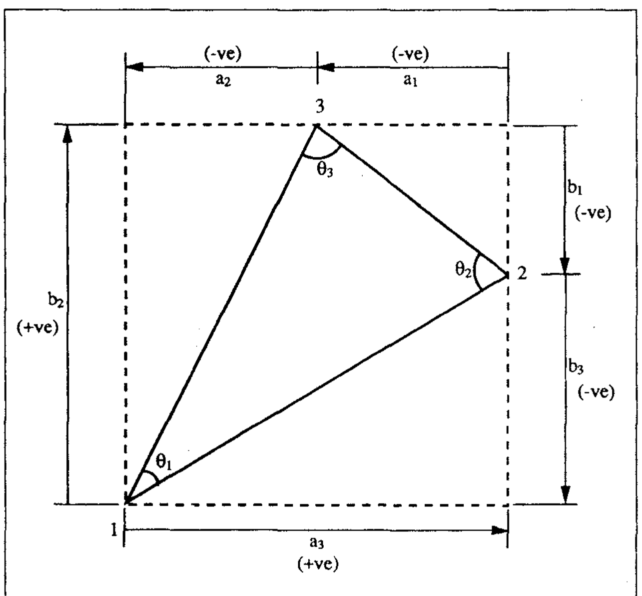

Fig. 3—Some definitions for the geometric factors in an element.

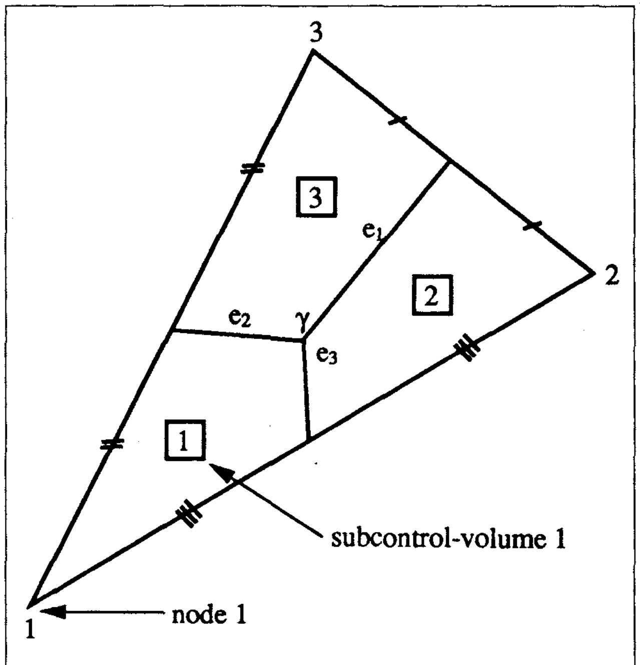

Fig. 2—Subcontrol volumes in a triangular element.

Similar expressions can be written for u_2 and u_3.

Thus, in matrix form,

$$\{u\}=\frac{1}{4A}[B]^T[k][B]\{\Phi\}, \quad \text{(12)}$$

which may be expanded to give

$$\{u\}=\begin{bmatrix} T_{12}^e+T_{13}^e & -T_{12}^e & -T_{13}^e \\ -T_{12}^e & T_{12}^e+T_{23}^e & -T_{23}^e \\ -T_{13}^e & -T_{23}^e & T_{13}^e+T_{23}^e \end{bmatrix}\{\Phi\}, \quad \text{(13)}$$

where $$T_{ij}^e=-\left(\frac{k_x b_i b_j+k_y a_i a_j}{4A}\right), \; i\neq j. \quad \text{(14)}$$

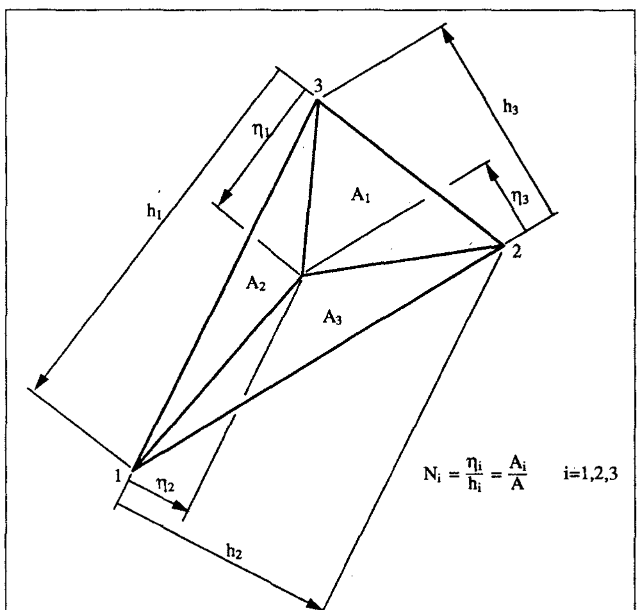

Fig. 4—Definitions of elemental interpolation functions.

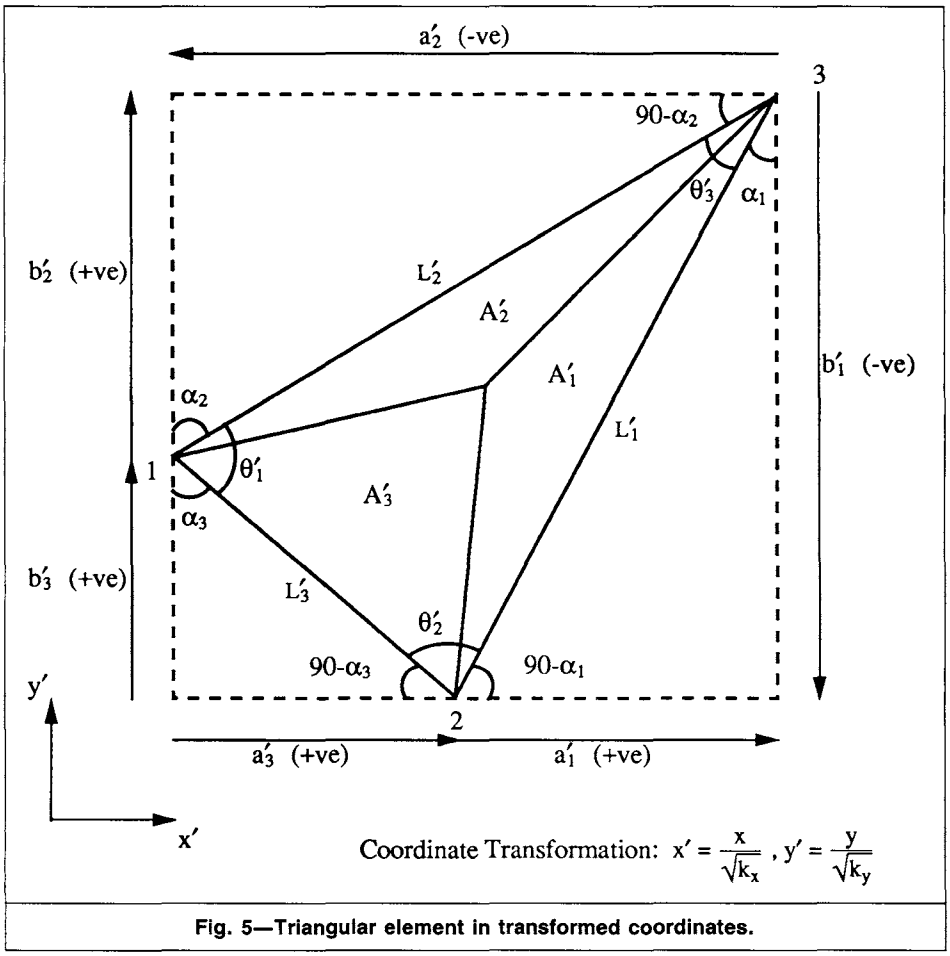

Fig. 5—Triangular element in transformed coordinates.

The transmissibility matrix in Eq. 13 is symmetric, with the diagonal elements equal to the negative row sum of the off-diagonal elements. The flow terms for each subcontrol volume are

$$u_1=-[T^e_{12}(\Phi_2-\Phi_1)+T^e_{13}(\Phi_3-\Phi_1)], \quad \ldots\ldots\ldots\ldots (15a)$$

$$u_2=-[T^e_{12}(\Phi_1-\Phi_2)+T^e_{23}(\Phi_3-\Phi_2)], \quad \ldots\ldots\ldots\ldots (15b)$$

and $$u_3=-[T^e_{13}(\Phi_1-\Phi_3)+T^e_{23}(\Phi_2-\Phi_3)]. \quad \ldots\ldots\ldots\ldots (15c)$$

Note that the CVFE discretization method produces equations that bear a strong resemblance to the traditional finite-difference equations, with different transmissibilities calculations.

The method for assembling the global transmissibility array now is considered. If γ is chosen to be the barycenter of the element (see Fig. 2) such that $A_1=A_2=A_3=A/3$, then the area occupied by a control volume can easily be calculated:

$$A_{CV_j}\sum_{i\epsilon\eta_i} A_{E_i}/3, \quad \ldots\ldots\ldots\ldots (16)$$

where η_i are all the finite elements with Node j.

Each connection between adjacent nodes will include contribution from the two elements sharing the common edge. The transmissibility between Nodes i and j, where at least either i or j is not on the external boundary, is

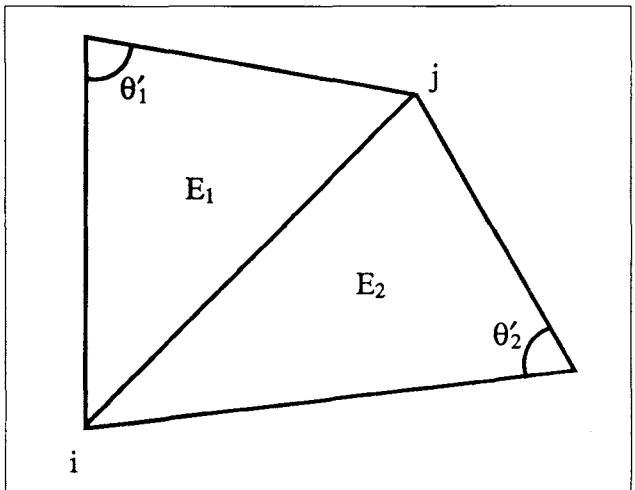

Fig. 6—Two adjacent elements in the transformed coordinates.

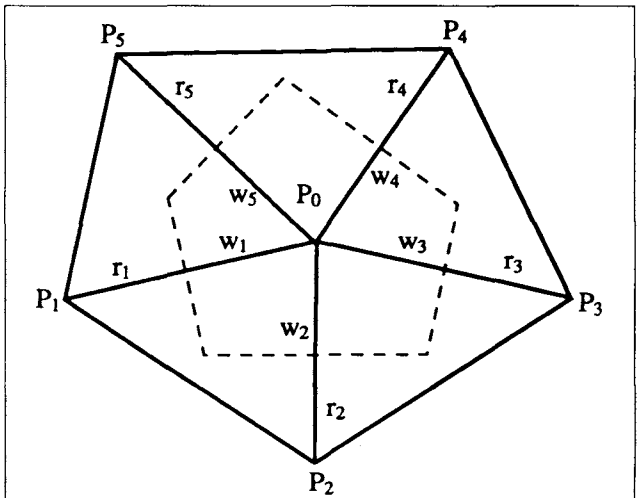

Fig. 7—Definitions of well control volume for the calculation of well index and equivalent well radius.

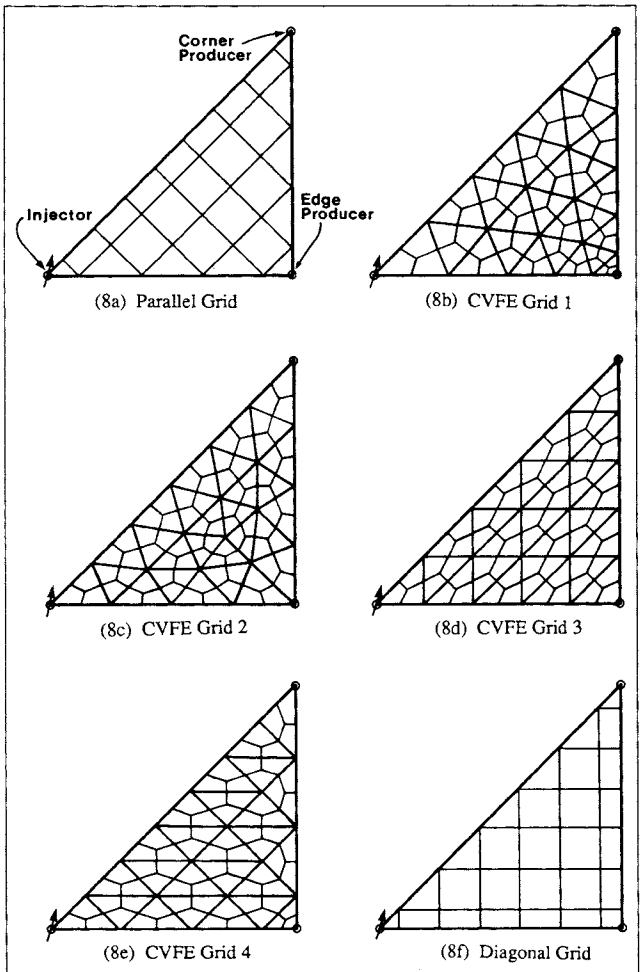

Fig. 8—Grids used for the first numerical example—SPE4 Problem 2.

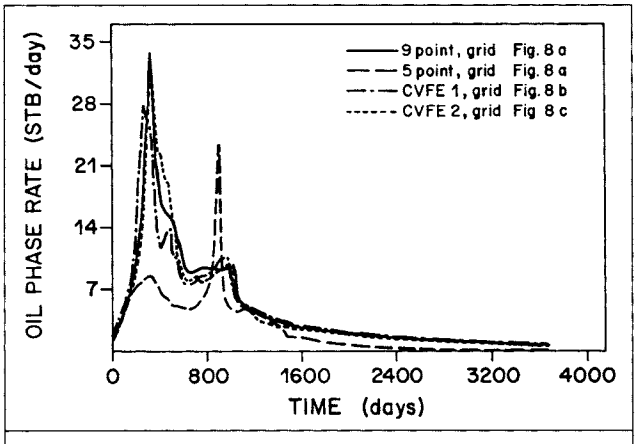

Fig. 9—Comparison of oil rates for the edge producer among CVFE, five-point, and nine-point difference methods.

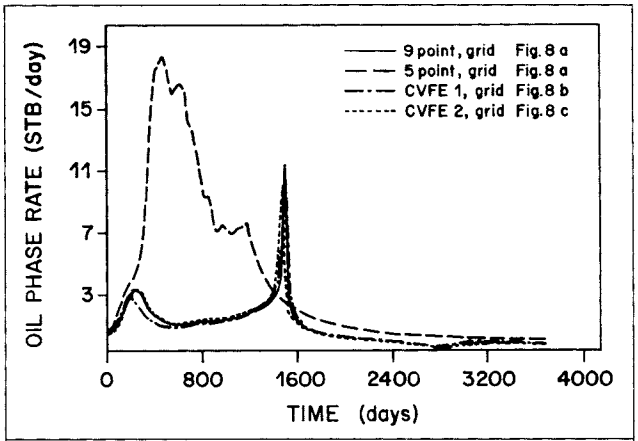

Fig. 10—Comparison of oil rates for the corner producer among CVFE, five-point, and nine-point difference methods.

$$T_{ij}^{g}=-\sum_{e=1}^{2}\left(\frac{k_{x_{ij}}b_i b_j+k_{y_{ij}}a_i a_j}{4A_{ij}}\right)_e \quad \ldots\ldots\ldots\ldots\ldots\ldots (17)$$

Note that the global transmissibility array need be calculated only once, with T_{ij}^{g} stored for subsequent timesteps and iterations. The global equation for each control volume can thus be written as

$$V_{T_i}\left[\frac{(\phi\rho)_i^{n+1}-(\phi\rho)_i^{n}}{\Delta t}\right]=\sum_{j\epsilon\xi_i}T_{ij}^{g}(\Phi_j-\Phi_i), \quad \ldots\ldots\ldots\ldots (18)$$

where V_{T_i} is the total volume of Control Volume i and ξ_i are all the neighboring nodes of i. For multiphase flow, the phase mobility, λ_P, can be added to the flow terms and evaluated with upstream weighting:

$$\lambda_P=\lambda_{Pi} \text{ if } \Phi_i>\Phi_j \quad \ldots\ldots\ldots\ldots\ldots\ldots\ldots\ldots (19a)$$

and $\lambda_P=\lambda_{Pj}$ if $\Phi_j>\Phi_i$. $\ldots\ldots\ldots\ldots\ldots\ldots\ldots\ldots (19b)$

Jacobian matrix construction for Eq. 18 can be done the same way as for the finite-difference method[13] because discretized equations from both methods leave similar forms. However, the proposed discretization technique provides considerable flexibility for treating problems with complex geometry. Triangulation can be performed over any irregularly shaped solution domain with smaller triangles in the region(s) where high resolution is desired.

In Appendix A, the CVFE method is shown to give the same discretized equation as the Petrov-Galerkin finite-element method for single-phase incompressible flow.

Positive Transmissibility Coefficient. A regularity condition needs to be imposed on the triangular mesh such that a negative transmissibility coefficient will not occur; i.e.,

$$T_{ij}>0,\ i\neq j. \quad \ldots\ldots\ldots\ldots\ldots\ldots\ldots\ldots\ldots\ldots (20)$$

It can be shown that

$$T_{ij}=\sqrt{k_x k_y}\left(\frac{L_i' L_j' \cos\theta_k'}{4A'}\right),\ i\neq j\neq k, \quad \ldots\ldots\ldots\ldots\ldots (21)$$

where L_i' and L_j' are the length of the sides of the element in the transformed coordinates,

$$x'=x/\sqrt{k_x} \quad \ldots\ldots\ldots\ldots\ldots\ldots\ldots\ldots\ldots\ldots (22a)$$

and $y'=y/\sqrt{k_y}$ $\ldots\ldots\ldots\ldots\ldots\ldots\ldots\ldots\ldots\ldots (22b)$

and θ_k' is the included angle shown in **Fig. 5.** Because each global transmissibility consists of contributions from two adjacent elements, the transmissibility between Nodes i and j in **Fig. 6** (assuming a homogeneous anisotropic medium) is

$$T_{ij}=\sqrt{k_x k_y}\left(\frac{\cot\theta_1'+\cot\theta_2'}{2}\right). \quad \ldots\ldots\ldots\ldots\ldots\ldots (23)$$

The requirement $T_{ij}>0$ is equivalent to

$$\theta_1'+\theta_2'<\pi, \quad \ldots\ldots\ldots\ldots\ldots\ldots\ldots\ldots\ldots\ldots (24)$$

where θ_1' and θ_2' are the opposite angles of Elements 1 and 2 in the transformed coordinates. Eq. 24 is the necessary and sufficient condition for positive transmissibility coefficients. For angles located on the external boundaries, the requirement becomes

$$\theta'<\pi/2. \quad \ldots\ldots\ldots\ldots\ldots\ldots\ldots\ldots\ldots\ldots (25)$$

TABLE 1—EXAMPLE 1—SPE4 PROBLEM 2

Cases	Timesteps	Iterations	Nodes/ Layer	Normalized Run Time*
Nine-point (Fig. 8a)	93	460	25	1.0
Five-point parallel (Fig. 8a)	87	445	25	0.726
Five-point diagonal (Fig. 8f)	112	543	28	0.996
CVFE Grid 1 (Fig. 8b)	88	434	21	0.707
CVFE Grid 2 (Fig. 8c)	87	420	22	0.726
CVFE Grid 3 (Fig. 8d)	89	450	21	0.671
CVFE Grid 4 (Fig. 8e)	113	585	21	0.829

*Obtained with an adaptive-implicit method.

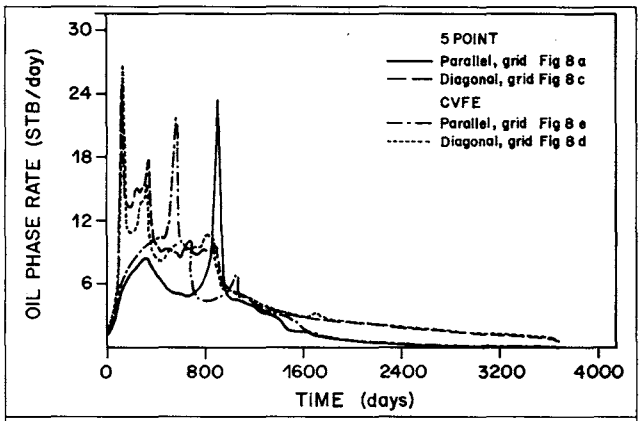

Fig. 11—Comparison of grid-orientation effects between two CVFE grids and the diagonal and parallel five-point difference grids—edge producer.

Ref. 14 gives additional details of this method. Rozon[15] reported an alternative CVFE method that uses quadrilateral elements. That method was later extended to solve the coupled geomechanic/multiphase-flow problem.[6] Except for the special case of rectangular elements, however, a matrix assembly procedure generally is required for the Jacobian construction of quadrilateral elements.

Grid Construction

The triangular mesh in this study is constructed by subdividing the reservoir into triangular subregions. These subregions are triangulated and then gathered to form the complete solution domain. The complete mesh is adjusted by a smoothing procedure with the reservoir boundary and the well locations remaining fixed. Mesh density can be adjusted to give higher resolution around the wells. The subregions are chosen such that there are no obtuse angles. The mesh thus generated satisfies Delaunay triangulation.[17] The smoothing procedure tends to preserve the empty circumcircle property of the original triangles. However, a swap test generally should be performed to preserve Delaunay triangles. The resulting mesh also is checked to observe the positive transmissibility constraints discussed earlier. In 3D cases, the third dimension is obtained by vertical projection of the 2D grid.

Well Representation

Following the notation of Peaceman,[18] the equivalent radius, r_0, of the control volume containing a well is defined as that radius at which steady-state flowing pressure for the actual well is equal to the numerically calculated pressure for the well control volume:

$$p_{wf}-p_0=\frac{q\mu}{2\pi kh}\ln\frac{r_w}{r_0}. \quad \ldots\ldots\ldots\ldots\ldots\ldots\ldots\ldots\ldots\ldots\ldots\ldots\ldots\ldots (26)$$

Referring to **Fig. 7,** the flow from adjacent control volumes to the control volume containing a well is assumed to satisfy the radial flow equation

$$p_i-p_0=\frac{q\mu}{2\pi kh}\ln\frac{r_i}{r_0}, \quad \ldots\ldots\ldots\ldots\ldots\ldots\ldots\ldots\ldots\ldots\ldots\ldots\ldots\ldots (27)$$

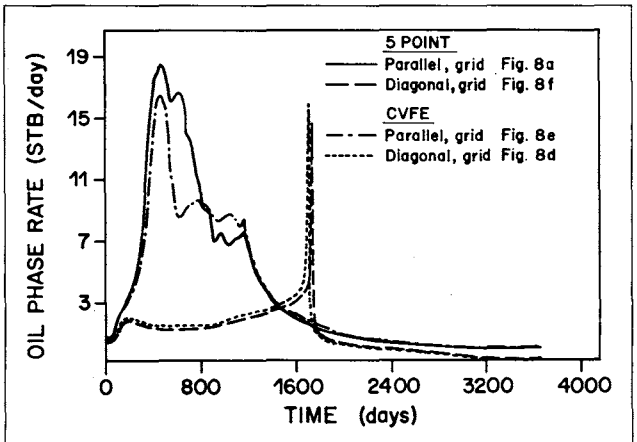

Fig. 12—Comparison of grid orientation effects between two CVFE grids and the diagonal and parallel five-point difference grids—corner producer.

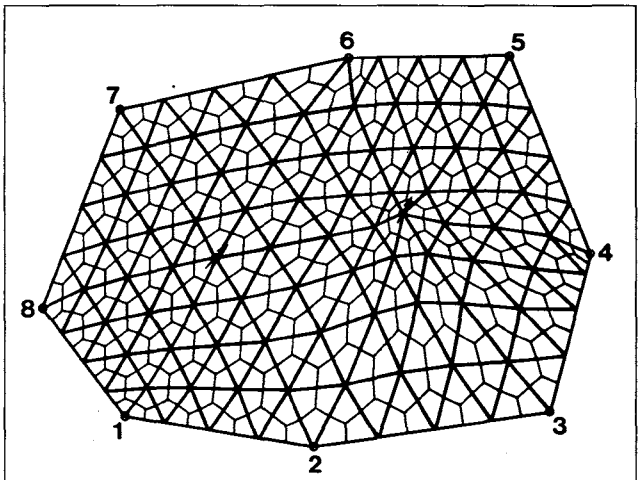

(13a) CVFE Grid

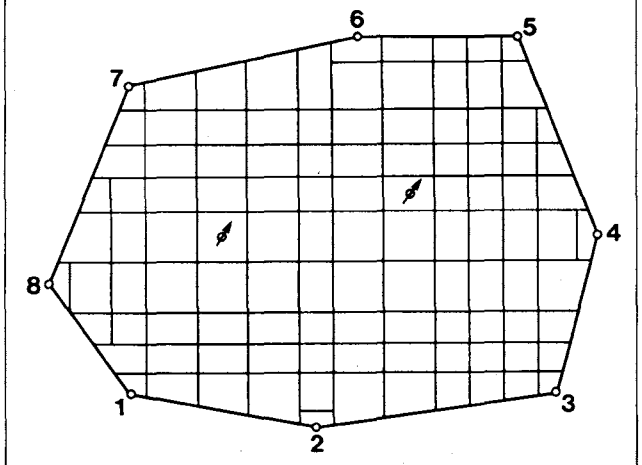

(13b) 9-point Cartesian Grid

Fig. 13—Grids for the second numerical examples.

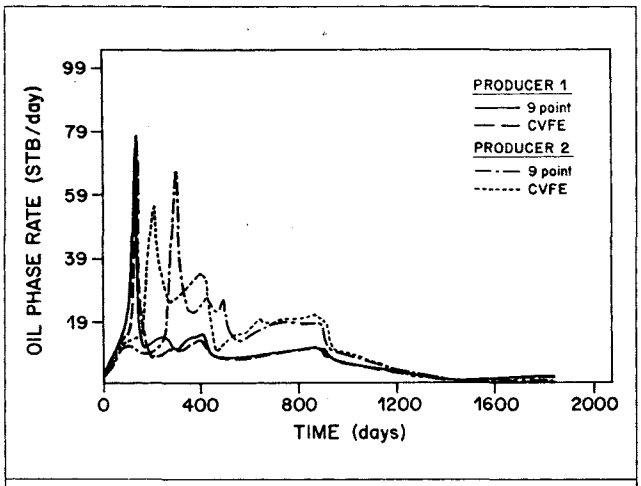

Fig. 14—Comparison of oil rates between the CVFE method and the nine-point method for Producers 1 and 2, Problem 2.

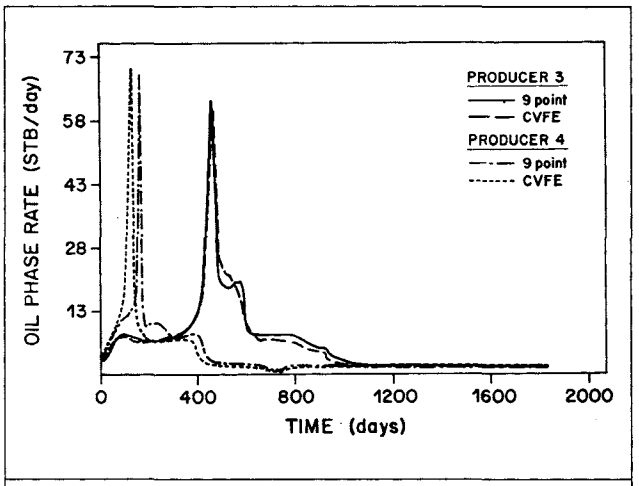

Fig. 15—Comparison of oil rates between the CVFE method and the nine-point method for Producers 3 and 4, Problem 2.

where $i \in$ adjacent nodes. The finite-difference equation for the steady-state pressure distribution for Control Volume 0 is

$$q=\frac{kh}{\mu}\left[\sum\frac{w_i}{r_i}(p_i-p_0)\right], \quad \ldots\ldots\ldots\ldots\ldots\ldots\ldots\ldots (28)$$

where w_i=width and r_i=radius, as shown in Fig. 7. Combining Eqs. 27 and 28 gives the equivalent radius, r_0:

$$r_0=e^{[(\Sigma\alpha_i \ln r_i-2\pi)/\Sigma\alpha_i]}, \quad \ldots\ldots\ldots\ldots\ldots\ldots\ldots\ldots (29)$$

where $\alpha_i=w_i/r_i$. Note that when $k_x \neq x_y$, r_0 should be calculated from the transformed plane $x'=x/\sqrt{k_x}$ and $y'=y/\sqrt{k_y}$, where the permeability is $k'=\sqrt{k_x k_y}$. The well index is therefore calculated as

TABLE 2—EXAMPLE 2—IRREGULAR-PATTERN STEAMFLOOD

Cases	Timesteps	Iterations	Nodes/ Layer	Normalized CPU Time*
Nine-point (Fig. 13b)	163	915	110	1.000
CVFE grid (Fig. 13a)	144	819	97	0.686

*Obtained with an adaptive-implicit method.

$$I_w=\frac{2\pi k'hf}{\left(\ln\frac{r_0}{r_w}+s\right)}, \quad \ldots\ldots\ldots\ldots\ldots\ldots\ldots\ldots\ldots\ldots (30)$$

where f=well fraction, s=skin factor, and h is the average thickness of Control Volume 0.

Thermal Reservoir Model

The CVFE method was implemented in an adaptive-implicit four-phase (oil, water, gas, and solid) multicomponent dual-porosity/dual-permeability thermal simulator.[19,20] This simulator can model a large number of thermal and isothermal EOR processes, including multicomponent steamdrive, in-situ combustion, foam, and chemical EOR. Both five-point and nine-point[21,22] block-centered discretization methods are available. The model uses an arbitrary connection solver, so implementation of the CVFE method was relatively straightforward. Appendix B briefly describes the modeling equations.

Numerical Examples

It is well known that the five-point finite-difference method has severe grid-orientation errors. This is particularly true for simulation involving miscible displacement, steamflood, and in-situ combustion processes. Nine-point schemes[21-23] were introduced to minimize grid-orientation errors. Although these methods were successful, computational cost also increased significantly. In this

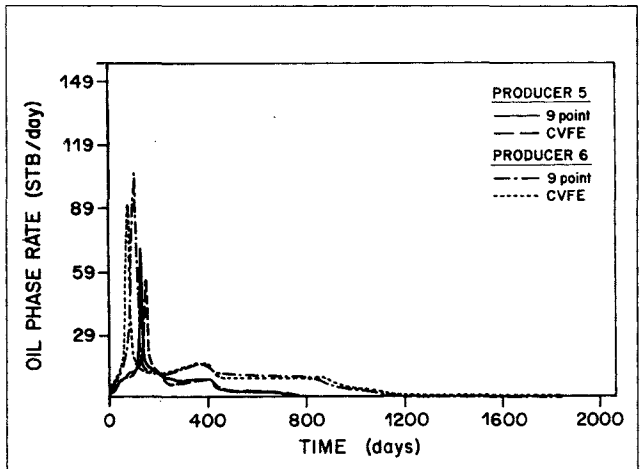

Fig. 16—Comparison of oil rates between the CVFE method and the nine-point method for Producers 5 and 6, Problem 2.

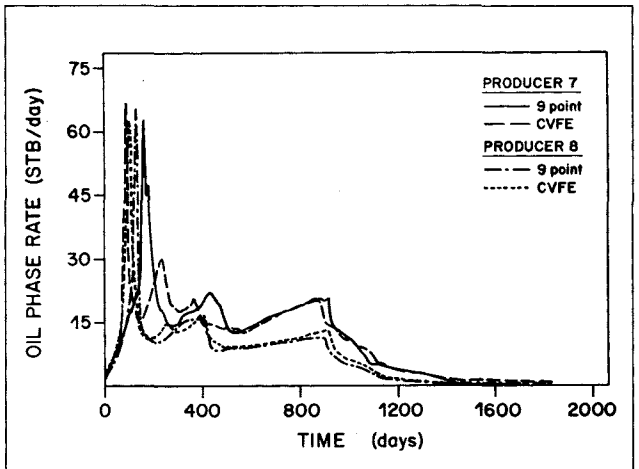

Fig. 17—Comparison of oil rates between the CVFE method and the nine-point method for Producers 7 and 8, Problem 2.

work, the grid-orientation sensitivity of the CVFE method is examined for two numerical examples.

Case 1—Fourth SPE Comparative Solution Project Problem 2. The second problem of the Fourth SPE Comparative Solution Project (SPE4) deals with steam displacement of heavy oil in a one-eighth element of symmetry of an inverted nine-spot pattern. The problem has four layers. The suggested finite-difference grid is $9\times5\times4$ (**Fig. 8a**). Ref. 24 gives the rock and fluid properties, as well as the operating conditions. The problem was known to show serious grid-orientation effects with five-point finite-difference schemes. Two CVFE grids (**Figs. 8b and 8c**) were used. The CVFE results are compared against nine-point and five-point simulations using the grid shown in Fig. 8a. The oil rates for the corner and edge producers for the various runs are shown in **Figs. 9 and 10.** Both CVFE simulations give results close to those of the nine-point run. **Table 1** gives the number of grid nodes, timesteps, and iterations, along with the normalized run time. Both CVFE simulations show favorable run times compared with the nine-point scheme.

To show grid-orientation effects with CVFE, two additional CVFE grids with right-angle triangles (**Figs. 8d and 8e**) were used to solve the same problem. Note that the triangles are rotated by 90° between the two figures. These results are compared against those obtained with the parallel grid (Fig. 8a) and the diagonal grid (**Fig. 8f**) with five-point differences. **Figs. 11 and 12** show the oil rates for the corner and edge producers. These runs show that the construction of a triangular mesh by dividing rectangular grids into right-angle triangles is not optimal and should be avoided, especially for problems involving unfavorable-mobility-ratio, piston-like displacements.

Case 2—Irregular-Pattern Steamflood. The second problem is an irregular-pattern steamflood in a reservoir with four layers tilted at 20° in the x direction. The CVFE grid and the corresponding finite-difference grid are shown in **Figs. 13a and 13b.** The finite-difference grid was adjusted to fit the irregular boundary by use of block-volume and area modifiers for all the boundary blocks. The rock and fluid properties are from Case 1. The two injectors are constrained to (1) a maximum bottomhole pressure (BHP) of 1,000 psia and (2) a maximum injection rate of 200 STB/D cold-water equivalent. The quality of the injected steam is 0.7 at 450°F. The producers are subjected to the following constraints: (1) minimum BHP of 17 psia, (2) maximum production rate of 1,000 STB/D of liquids, and (3) maximum steam rate of 10 STB/D.

Figs. 14 through 17 compare the oil rates of the CVFE method and the nine-point difference method for the eight producers. The biggest differences between the two runs were the breakthrough times for Producers 2 and 7. The recovery behaviors of the two methods for the entire simulation period are almost identical. **Table 2** gives the run time, timestep, and iteration information. The CVFE simulation uses 97 nodes, vs. 110 active nodes for the nine-point simulation.

Observations. It is found that, to minimize grid-orientation effects, the aspect ratio (defined as the ratio of the longest element side to the shortest element side) of the triangular elements in the transformed plane ($x'=x/\sqrt{k_x}$, $y'=y/\sqrt{k_y}$) should be minimized. Generally, if an aspect ratio of unity cannot be used throughout, then a random orientation of triangles is preferred over a regular structure. As the current results indicate, however, the effort required to produce grids that are substantially insensitive to grid orientation is relatively small and the computational costs for the cases tested are significantly less than those for a nine-point scheme. These results, combined with the geometric flexibility and ease of integration into existing reservoir simulators, suggest that the CVFE method would be a very useful technique for reservoir simulation.

Conclusions

A discretization procedure that uses the CVFE method has been developed. The method has the following advantages.

1. The CVFE conservation equations can be converted to the same form as the finite-difference equations. Implementation of the method into existing reservoir simulators is straightforward.
2. Triangular elements may be used to fit into any geometrically complex solution domain.
3. Local grid refinement can be performed consistently. There is no special technique required to reduce discretization errors at the coarse-grid/fine-grid boundary.
4. The resulting matrix can be solved efficiently with an arbitrary connectivity solver. There is minimal increase in computer time and storage associated with the method. The geometric flexibility introduced can provide great savings by concentrating gridpoints only where they are needed.

The method has been implemented into a general-purpose thermal simulator. Our test results indicate that grid-orientation errors can be reduced substantially by choosing proper triangular elements. The method is shown to give the same discretized equations as the Petrov-Galerkin finite-element method for single-phase incompressible flow. The criterion for positive transmissibility coefficient in anisotropic reservoirs also is derived.

Nomenclature

a_1,a_2,a_3,
b_1,b_2,b_3 = geometric factors for elemental derivation
A = area
e_1,e_2,e_3 = subcontrol-volume boundaries
f = well fraction
h = thickness
H = fluid enthalpy
I_w = well index
k = permeability
k_h = thermal conductivity
L_1,L_2,L_3 = lengths of finite-element sides
n_c = number of components
n_P = number of phases
n_{rx} = number of reactions
N_i = interpolation function
p = pressure
p_{wf} = bottomhole flowing pressure
p_0 = pressure at Control Volume 0
P_c = capillary pressure
q = flow rate
q_E = injection/production of energy
q_m = injection/production of mass
Q_{ext} = energy sink/source from external heaters
Q_{loss} = heat loss to overburden and underburden
r_i = radial length i
r_w = wellbore radius
r_0 = equivalent radius
R = reaction component sink/source term
R_u = reaction heat sink/source term
s = skin factor
S = saturation
t = time
T = transmissibility
T_r = reference temperature
u = flux
U = internal energy
V_i = volume of Gridblock i
w_i = flow width i
W_i = weighting functions
x = coordinate or mole fraction
y = coordinate
α_i = w_i/r_i ratio
θ = angle
λ = mobility, kr/μ
μ = viscosity
ρ = molar density
$(\rho c_p)_r$ = rock heat capacity

ϕ = porosity
Φ = potential

Subscripts

b = block
CV = control volume
ic = component
i,j,k = indices
irx = reaction
P = phase
r = rock
t = total

Superscripts

e = element
g = global
n = timestep n
T = transpose
$\rightarrow$ = vector

Acknowledgment

This research was supported by the members of the Computer Modelling Group. We thank J. Grabenstetter for useful discussions during the course of this research.

References

1. Wadsley, W.A.: "Modeling Reservoir Geometry With Non-Rectangular Coordinate Grids," paper SPE 9369 presented at the 1980 SPE Annual Technical Conference and Exhibition, Dallas, Sept. 21-24.
2. Goldthorpe, W.H. and Chow, Y.S.: "Unconventional Modeling of Faulted Reservoirs: A Case Study," paper SPE 13526 presented at the 1985 SPE Reservoir Simulation Symposium, Dallas, Feb. 10-13.
3. Forsyth, P.A. and Sammon, P.H.: "Local Mesh Refinement and Modeling of Faults and Pinchouts," *SPERE* (June 1986) 275-85.
4. Heinemann, Z.E., Gerken, G., and Hantelmann, G.: "Using Grid Refinement in Multiple-Application Reservoir Simulator," paper SPE 12255 presented at the 1983 SPE Reservoir Simulation Symposium, San Francisco, Nov. 15-18.
5. Quandalle, P. and Besset, P.: "Reduction of Grid Effects Due to Local Sub-Gridding in Simulations Using a Composite Grid," paper SPE 13527 presented at the 1985 SPE Reservoir Simulation Symposium, Dallas, Feb. 10-13.
6. Pedrosa, O.A. and Aziz, K.: "Use of Hybrid Grid in Reservoir Simulation," *SPERE* (Nov. 1986) 611-21; *Trans.*, AIME, **282.**
7. Huyakorn, P.S. and Pinder, G.F.: "A Pressure-Enthalpy Finite Element Model for Simulating Hydrothermal Reservoirs," *Advances in Computer Methods for Partial Difference Equations II*, R. Vichnevetsky (ed.), IMACS (AICA) (1977) 284-93.
8. Baliga, B.R. and Patankar, S.V.: "A New Finite-Element Formulation for Convection-Diffusion Problems," *Num. Heat Trans.* (1980) **3,** 393-409.
9. Schneider, G. and Raw, M.J.: "A Skewed, Positive Influence Coefficient Upwinding Procedure for Control Volume Based Finite Element Convection Diffusion Computation," *Num. Heat Trans.* (1986) **9,** 1-26.
10. Heinemann, Z.E. and Brand, C.: "Modeling Reservoir Geometry With Irregular Grids," *SPERE* (May 1991) 225-32; *Trans.*, AIME, **291.**
11. Pruess, K. and Bodvarsson, G.S.: "A Seven-Point Finite-Difference Method for Improved Grid Orientation Performance in Pattern Steamfloods," paper SPE 12252 presented at the 1983 SPE Reservoir Simulation Symposium, San Francisco, Nov. 16-18.
12. Forsyth, P.A.: "A Control-Volume Finite-Element Method for Local Mesh Refinement," *SPERE* (Nov. 1990) 561-66; *Trans.*, AIME, **289.**
13. Au, A. *et al.*: "Techniques for Fully Implicit Reservoir Simulation," paper SPE 9302 presented at the 1980 SPE Annual Technical Conference and Exhibition, Dallas, Sept. 21-24.
14. Fung, L.S.-K. and Nghiem, L.X.: "A Control-Volume Finite-Element Scheme Using Triangular Elements for Reservoir Simulation," CMG Report 90.03.R, Calgary (March 1990).
15. Rozon, B.J.: "A Generalized Finite-Volume Discretization Method for Reservoir Simulation," paper SPE 18414 presented at the 1989 SPE Reservoir Simulation Symposium, Houston, Feb. 6-8.
16. Fung, L.S.-K.: "A Coupled Geomechanic-Multiphase Flow Model for the Analysis of In-Situ Recovery in Cohesionless Oil Sands," paper CIM 90-29, presented at the 1990 CIM/SPE Intl. Technical Meeting, Calgary, June 10-13.
17. Green, P.J. and Sibson, R.: "Computing Dirichlet Tessellations in the Plane," *Computer J.* (1978) **21,** 168-73.
18. Peaceman, D.W.: "Interpretation of Well-Block Pressures in Numerical Reservoir Simulation," *SPEJ* (June 1978) 183-94; *Trans.*, AIME, **265.**
19. Rubin, B. and Buchanan, W.L.: "A General Purpose Thermal Model," *SPEJ* (April 1985) 202-14.
20. Oballa, V., Coombe, D.A., and Buchanan, W.L.: "Adaptive-Implicit Method in Thermal Simulation," *SPERE* (Nov. 1990) 549-54.
21. McCracken, T.A. and Yanosik, J.L.: "A Nine-Point, Finite-Difference Reservoir Simulator for Realistic Prediction of Adverse Mobility Ratio Displacement," *SPEJ* (Aug. 1979) 253-62; *Trans.*, AIME, **267.**
22. Coats, K.H. and Modine, A.D.: "A Consistent Method for Calculating Transmissibility in Nine-Point Difference Equations," paper SPE 12248 presented at the 1983 SPE Reservoir Simulation Symposium, San Francisco, Nov. 15-18.
23. Shiralkar, G.S. and Stephenson, R.E.: "A General Formulation for Simulating Physical Dispersion and a New Nine-Point Scheme," *SPERE* (Feb. 1991) 115-120.
24. Aziz, K., Ramesh, A.B., and Woo, P.T.: "Fourth SPE Comparative Solution Project: Comparison of Steam Injection Simulators," *JPT* (Dec. 1987) 1576-84.

Appendix A—Discrete Equation for Single-Phase Flow, Petrov-Galerkin Method

The following derivation shows that the CVFE method produces the same discretized equation as the Petrov-Galerkin finite-element method for single-phase incompressible flow. The Petrov-Galerkin method is a form of weighted residual method that satisfies

$$\iint_{\Omega} W_i R \mathrm{d}\Omega = 0, \quad \ldots\ldots\ldots\ldots\ldots\ldots\ldots\ldots\ldots\ldots \text{(A-1)}$$

where R is the conservation equation in residual form and the W_i are weighting functions taken to be the same as the interpolation functions, N_i, in the Petrov-Galerkin method. For the single-phase incompressible problem,

$$\iint_{\Omega} W_i \nabla\cdot(k\nabla\Phi)\mathrm{d}\Omega = 0. \quad \ldots\ldots\ldots\ldots\ldots\ldots\ldots\ldots\ldots\ldots \text{(A-2)}$$

Using integration by parts, Eq. A-2 becomes

$$\iint_{\Omega} \nabla W_i k \nabla\Phi \mathrm{d}\Omega + \int_{\Gamma} W_i k \nabla\Phi \mathrm{d}\Gamma = 0, \quad \ldots\ldots\ldots\ldots\ldots\ldots\ldots\ldots \text{(A-3)}$$

where Γ is the element boundary. Note that the second term in Eq. A-3 will disappear upon assembly of the global stiffness matrix as the fluxes across element boundaries cancel one another. Substituting the N_i and their derivatives into the first term of Eq. A-3 yields

$$\iint_{\Omega} \left(\frac{\partial N_i}{\partial x} k_x \frac{\partial N_i}{\partial x} \Phi_i + \frac{\partial N_i}{\partial y} k_y \frac{\partial N_i}{\partial y} \Phi_i \right) \mathrm{d}x\mathrm{d}y = 0. \quad \ldots\ldots\ldots\ldots \text{(A-4)}$$

Making use of Eq. 10, Eq. A-3 may be rewritten in matrix form as

$$\frac{1}{4A}[B]^T[k][B]\{\Phi\} = 0. \quad \ldots\ldots\ldots\ldots\ldots\ldots\ldots\ldots\ldots\ldots \text{(A-5)}$$

The same result was obtained for the CVFE method (see Eq. 12), and of course, the net inflow, u, is zero because, for the incompressible flow problem, the storage within a volume is constant.

Appendix B—Thermal Simulation Equations

The basic equations used in thermal simulation are the mass- and energy-conservation equations. Mass conservation is expressed in terms of components; the energy equation is the total energy balance.

Mass balance for Component ic that exists in n_P phases is

$$\sum_{p=1}^{n_P} \underbrace{\Delta[T\rho_P\lambda_P x_{Pic}(\Delta p+\Delta P_{cP}-\gamma_P\Delta z)]}_{\text{flow term}} =$$

$$\underbrace{\frac{V}{\Delta t}\Delta_t \sum_{P=1}^{n_P} \phi\rho_P S_P x_{Pic}}_{\text{accumulation}} + \underbrace{\sum_{irx=1}^{n_{rx}} R_{irx,ic}}_{\text{reaction}} + \underbrace{q_{m,ic}}_{\substack{\text{injection/}\\ \text{production}}} \quad \ldots\ldots\ldots \text{(B-1)}$$

The total energy balance is

$$\sum_{P=1}^{n_P} \underbrace{\Delta[T\rho_P\lambda_P H_P\cdot(\Delta p+\Delta P_{cP}-\gamma_P\Delta z)]}_{\text{flow term}} + \underbrace{\Delta(k_h\Delta T)}_{\substack{\text{thermal}\\ \text{conduction}}} =$$

$$\underbrace{\frac{V}{\Delta t}\Delta_t}_{\text{fluid accumulation}}\Bigg[\underbrace{\sum_{P=1}^{n_P} \phi\rho_P S_P U_P}_{\text{fluid accumulation}} + \underbrace{(1-\phi)(\rho c_P)_r(T-T_r)}_{\text{rock accumulation}}\Bigg] +$$

$$\underbrace{\sum_{irx=1}^{n_{rx}} R_{u,irx}}_{\text{reaction}} + \underbrace{q_E}_{\substack{\text{injection/}\\ \text{production}}} + \underbrace{Q_{\text{loss}}}_{\text{heat loss}} + \underbrace{Q_{\text{ext}}}_{\substack{\text{external}\\ \text{heaters}}} \quad \ldots\ldots\ldots \text{(B-2)}$$

In addition to the conservation equations, there is a saturation or gas-mole-fraction constraint equation that may be solved simultaneously with the reservoir flow equations.

SI Metric Conversion Factors

bbl	× 1.589 873	E−01	= m^3
°F	(°F−32)/1.8		= °C
psi	× 6.894 757	E+00	= kPa

SPERE

Original SPE manuscript received for review Feb. 17, 1991. Revised manuscript received Nov. 21, 1991. Paper accepted for publication Dec. 15, 1991. Paper (SPE 21224) first presented at the 1991 SPE Reservoir Simulation Symposium held in Anaheim, Feb. 17–20.

Authors

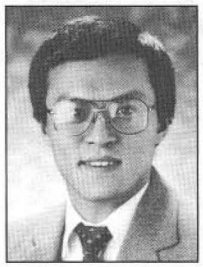
Fung


Hiebert


Nghiem

Larry S.-K. Fung is a staff engineer with the Computer Modelling Group (CMG) in Calgary. Since joining CMG in 1985, he has worked on several reservoir simulation R&D projects, including naturally fractured reservoir modeling, adaptive-implicit method, coupled geomechanical reservoir modeling, and flexible gridding methods. He previously was a research associate in compositional fluid mechanics at the U. of Alberta. Fung holds BS and MS degrees from the U. of Alberta. **Allan D. Hiebert,** a senior engineer at CMG, holds a PhD degree in electrical engineering from the U. of Alberta. His PhD research project was on the numerical simulation of electrical heating of oil-sand formations. Since joining CMG in 1985, he has worked in thermal and black-oil simulation and the development of input/output systems. He currently is working on the matrix solver AIMSOL and researching numerical methods. **Long X. Nghiem** is director of R&D for CMG. He joined the organization in 1977 and has been involved in various aspects of reservoir simulation: black-oil, compositional, thermal simulator development; phase-behavior calculations; sparse linear solver; fractures; and wellbore flow models. A member of the Editorial Review Committee, Nghiem also has served on the program committees for two Reservoir Simulation symposia. He holds degrees in chemical engineering from the U. of Montreal and the U. of Waterloo.